J Mater Sci (2010) 45:46–50
DOI 10.1007/s10853-009-3886-9

PEG-directed hydrothermal synthesis of alumina nanorods with mesoporous structure via AACH nanorod precursors

Zhenfeng Zhu · Hongjun Sun · Hui Liu · Dong Yang

Received: 26 June 2009 / Accepted: 11 September 2009 / Published online: 3 November 2009

Abstract Al_2O_3 nanorods with mesoporous structures are successfully synthesized from a hydrothermal and thermal decomposition process via the ammonium aluminum carbonate hydroxide (denoted as AACH) precursors. TEM images show that the average diameter of Al_2O_3 nanorods is about 60 nm, and the length is around 1–2 μm. The experimental results show that well-crystallized mesopores with hierarchically distributed pore sizes are embedded in the Al_2O_3 nanorods. The N_2 adsorption–desorption experiment indicates that the as-synthesized alumina nanorods have large surface area (ca. 176 m^2/g) and narrow pore-size distributions. At the same time, the as-prepared Al_2O_3 nanorods exhibit strong photoluminescent properties at room temperature. A plausible surfactant-induced nanorod formation mechanism using the poly ethylene glycols as the template agent for the nanorod assembly is also proposed.

Introduction

Alumina has been extensively used as advanced catalysts, catalyst supports [1], and adsorbents [2] because of its high specific surface and large pore volume [3]. However, the potential applications of aluminum oxide depend not only on its porosity, but also on its morphology [4]. For example, one-dimensional (1D) alumina nanostructures have received considerable interest due to their novel properties, such as high dielectric constant, good thermal and chemical stability, and high mechanical modulus [5, 6]. Other strategies for synthesis of alumina nanorods or nanowires include thermal evaporation method [7], electrochemical synthesis method [8], normal and lateral stepwise anodization [9], and sol–gel [10]. However, to our knowledge, high reaction temperatures, complex process control or long synthesis time may be required for these approaches. The introduction of hydrothermal process has provided a relatively simple and powerful method of the synthesis of 1D nanostructures [11]. Lee et al. synthesized alumina nanotubes, nanofibers, and nanorods based on templating of surfactants by hydrothermal reaction at 473 K for 72 h [12]. Zhu et al. reported the synthesis of alumina with a fiber morphology and large porosity using alumina hydrate with poly (ethylene oxide) (PEO) surfactant [13]. Zhang et al. designed a three-step synthesis route for preparation of lathlike and rod-shaped mesoporous alumina nanoparticles [14].

Herein, we report a facile hydrothermal method to synthesize alumina nanorods with mesoporous structures via ammonium aluminum carbonate hydroxide (AACH) precursor. The uniform AACH nanorods are synthesized by using PEG2000-directed hydrothermal method, in which the PEG2000, namely poly ethylene glycols (M_w 2000), which has been normally used as a templating agent to formation of 1D micro and nanostructures [15–18], was used as a template. Then, the AACH precursor is conveniently converted into the corresponding alumina nanorods with mesoporous structures followed by a calcination process without deformation of the microstructures.

Experimental

All chemicals are analytical-grade reagents without further purification; in a typical experiment, 0.1 mmol of PEG2000 was dissolved in 8 mL deionized water to form a transparent

Z. Zhu (✉) · H. Sun · H. Liu · D. Yang
School of Materials Science and Engineering, Shaanxi University of Science and Technology, Xi'an 710021, People's Republic of China
e-mail: zhuzf@sust.edu.cn; nmlab@sust.edu.cn

solution. Then, 5 mmol $Al(NO_3)_3 \cdot 9H_2O$ was added to the above solution under vigorous stirring. At last, an amount of urea was added into the above solution, giving rise to milky precipitates at pH ~5. The obtained precipitates were then transferred into a Teflon-lined autoclave of 40-mL capacity. The autoclave was heated to 80–160 °C for 24 h. After being cooled to room temperature, the white powders were collected and washed several times with distilled water to remove the impurities, and then, dried at 80 °C in a vacuum oven for 24 h. In order to study the phase transformation, calcination was also conducted at 900 and 1200 °C in a temperature-programmed Muffle furnace, respectively.

The crystalline phases of the alumina samples were characterized using X-ray diffraction (XRD-D/max2200pc, Japan) technique with Cu Kα radiation of wavelength $\lambda = 0.15418$ nm. The microscopic features of the as-synthesized and calcined alumina were characterized with transition electron microscope (TEM) and high resolution transition electron microscope (HRTEM) images (JEM 2010 from JEOL, Japan) operated at 200 kV. Thermogravimetric and differential thermal analyses (TGA–DTA) were conducted on a thermogravimetric analyzer, TGA 2050 (DTG-60AH SHIMADZU, Japan), with an air flow rate of 30 mL/min at a heating rate of 10 °C/min. The nitrogen adsorption isotherms and special surface areas were obtained using a Quantachrome Nova2000e surface area and pore size analyzer. The special surface areas were calculated using the Brunauer–Emmett–Teller (BET) model from a linear part of BET plot ($P/P_0 = 0.10$–0.30). Average pore diameters were calculated using the Barrett–Joyner–Halenda (BJH) method from the desorption branch of isotherm. Fourier transform infrared (FTIR) spectrometer (JASCO FT/IR-470, Japan) was used for detection of the AACH precursor and the alumina nanorods. Photoluminescent analyses (PL) were performed with an F-4500 spectrophotometer (Hitachi).

Results and discussions

Curve a in Fig. 1 shows the typical XRD pattern of the as-synthesized sample prepared at 140 °C for 24 h. All the peaks can be readily indexed as crystalline AACH with a composition of $NH_4[Al(OOH)HCO_3]$ (JCPDS card no. 42-0250) [19], which is conventionally synthesized by reaction of aluminum sulfate with ammonium hydrogen carbonate in the liquid phase. The high intensity of the XRD peaks of the as-synthesized sample indicated that the AACH phase synthesized in this study is highly crystalline. And just recently, we reported the synthesis of AACH microfibers using PEG6000 as template under hydrothermal conditions [20]. However, there are no reports available on the synthesis of AACH using PEG2000 as surfactant. After calcination at 900 °C for 2 h (Curve b in Fig. 1), the γ-Al_2O_3 phase

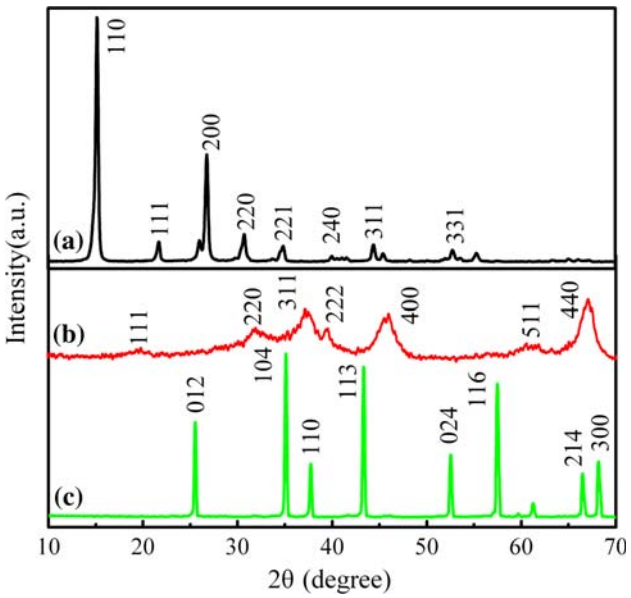

Fig. 1 XRD patterns of AACH samples prepared at 140 °C for 24 h (*a*); together with its respective conversion to γ-Al_2O_3 sample (*b*) at 900 °C for 2 h and α-Al_2O_3 sample (*c*) at 1200 °C for 2 h

(JCPDS card no. 10-0425) was observed. The low intensity of the XRD peak exhibited the alumina sample calcined at this temperature has a low crystallinity.Increasing further the calcination temperature to 1200 °C (Curve c in Fig. 1), the α-Al_2O_3 phase (JCPDS card no. 46-1212) was observed. The alumina sample has a high crystallinity, and the measured lattice constants of *a* and *c* of this hexagonal phase are 4.763 and 12.029 Å, respectively, which is in good agreement with theoretical values ($a = b = 4.759$ and $c = 12.993$ Å, respectively). No other diffraction peaks were detected, indicating that no impurity exists and the precursors have completely transformed into the α-Al_2O_3 phase.

In order to explore the thermolysis behavior of the as-prepared precursor AACH nanorods into alumina nanorods, we carried out the thermogravimetric analysis and differential scanning calorimetry (TG–DSC). Test conditions were started from 25 to 1300 °C at a rate of 10 °C/min in a flowing nitrogen environment. It is well known that $NH_4[Al(OOH)HCO_3]$ (AACH) is converted to alumina by release of H_2O, NH_3, and CO_2 with the elevating temperature, as described in the following equation [21]:

$$NH_4[Al(OOH)HCO_3] \rightarrow AlOOH + CO_2\,(31.65\ \text{mass loss}\,\%) + NH_3\,(12.23\ \text{mass loss}\,\%) + H_2O\,(12.95\ \text{mass loss}\,\%) \quad (1)$$

$$2AlOOH \rightarrow Al_2O_3 + H_2O \quad (2)$$

Combining the above reactions yields an overall reaction:

$$2NH_4[Al(OOH)HCO_3] \rightarrow Al_2O_3 + 2CO_2\,(31.65\,\text{mass loss}\,\%) + 2NH_3\,(12.23\,\text{mass loss}\,\%) + 3H_2O\,(19.42\,\text{mass loss}\,\%) \quad (3)$$

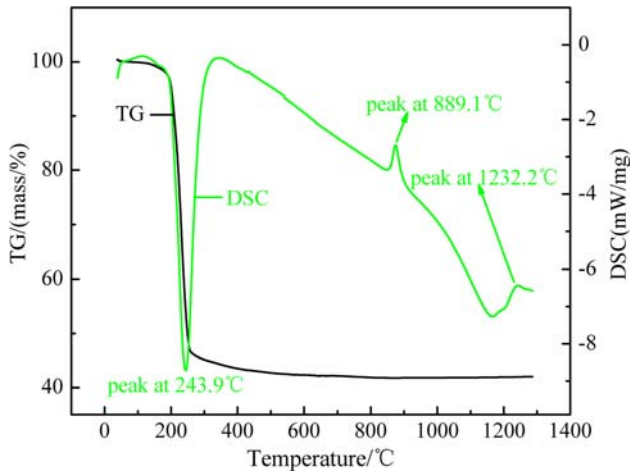

Fig. 2 TG–DSC plot of the AACH precursor

The TG–DSC curves of the precursor are shown in Fig. 2. The TGA curve shows that the sample has two major weight loss events. The first weight loss below 180 °C is due to the desorption of physically adsorbed water. The second weight loss event in the temperature range of 170–250 °C, which also can be seen from the aculeated exothermic peak at 243 °C of the DSC curve, is associated with the decomposition of PEG2000, together with the decomposition of AACH, releasing CO_2, NH_3, and H_2O and forming AOOH particles. With the increase of the temperature in the thermal process, the TGA curve keep also on slightly decreasing, indicating the decomposition of AACH and forming the alumina particles. It is worth mentioning that the DSC plot presents two endothermic peaks at 889 and 1232 °C, respectively. They maybe associated with the phase transition process of the alumina.

TEM analysis was conducted to vividly depict the characteristics of samples. Figure 3a show the TEM images of AACH nanorods prepared at 140 °C for 24 h with low magnification. The samples consists of a large number of nanorods with a length of 1 ~ 2 μm. In order to characterize the intrinsic structure of the AACH nanorods, we carried out the HRTEM analysis. Figure 3b depicts an individual AACH nanorod with the average width of 80 nm. The selected area electron diffraction (SAED) pattern (the inset of Fig. 3b) indicates that AACH nanorods always exhibit the same single-crystalline pattern. Figure 3c–e exhibit the TEM images and SAED pattern of γ-Al_2O_3 nanorods prepared by calcination of AACH nanorods at 900 °C for 2 h. Compared with the TEM image Fig. 3b, we can see from Fig. 3d that the calcined alumina nanorods are relatively small in diameter (about 60 nm) and more porous. This is probably induced by the completely release of H_2O and decomposition of PEG and AACH precursor. The inset SAED pattern in Fig. 3d indicates that γ-Al_2O_3 nanorods exhibit polycrystalline pattern. Figure 3e give us the amplified HRTEM images with the lattice spacing of 0.28 nm, in accordance with that of (220) plane of γ-Al_2O_3 sample.

In order to give further insight into the porous structure and the pore size distribution of the as-obtained production, the Brunauer–Joyner–Halenda (BJH) measurement was performed to examine the characteristic of pores. Figure 4 presents the typical N_2 adsorption–desorption isotherms and pore size distributions of the product calcined at 900 °C. It

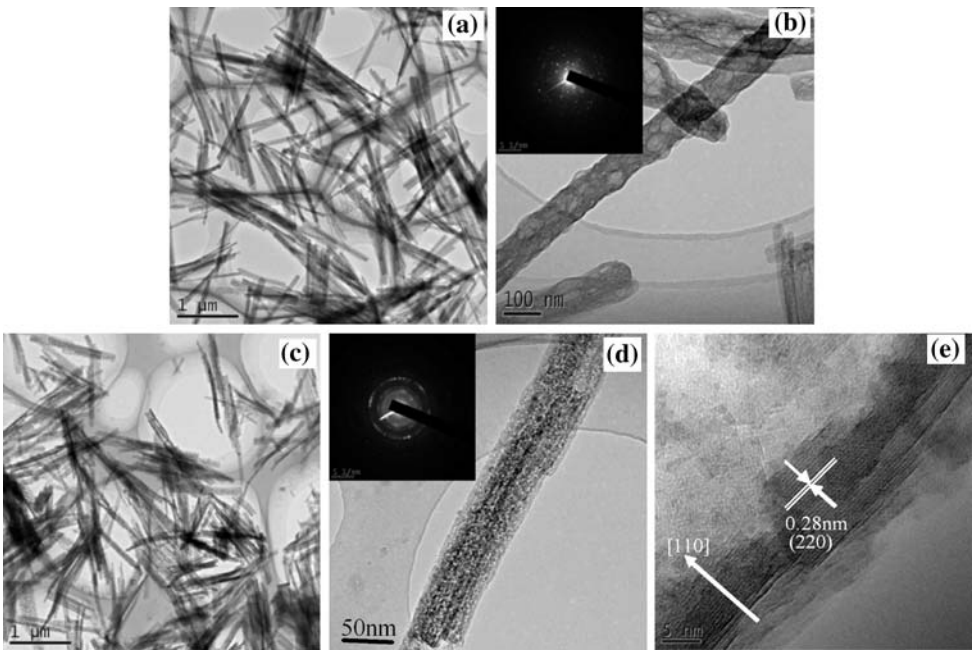

Fig. 3 **a**, **b** TEM images of AACH nanorods prepared at 140 °C for 24 h; **c–e** TEM images of γ-Al_2O_3 nanorods prepared by calcination of AACH nanorods at 900 °C for 2 h

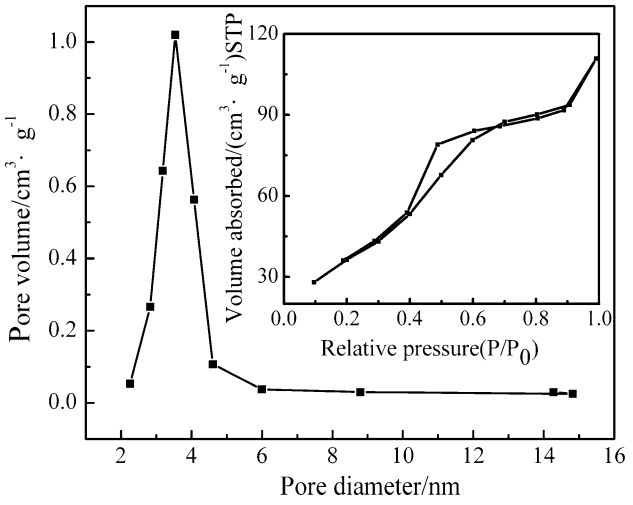

Fig. 4 N_2 absorption and desorption isotherms (*insets*) and pore-size distributions of the γ-Al_2O_3 nanorods

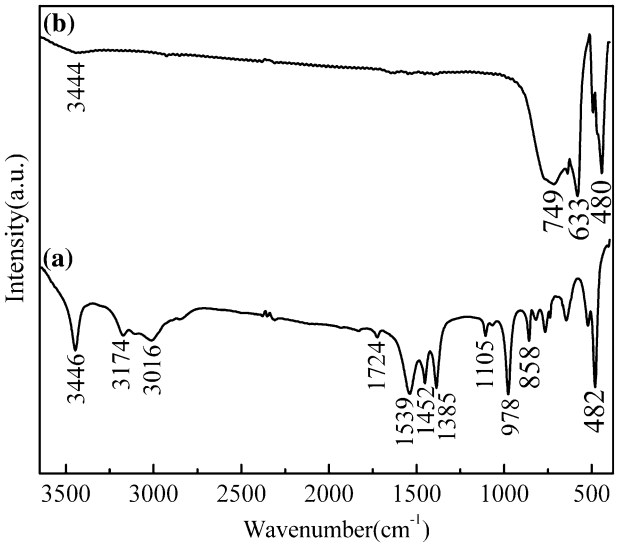

Fig. 5 FTIR spectra of (*a*) the precursor AACH and (*b*) Al_2O_3 obtained by calcination at 900 °C

is obvious that the pore diameter distribution of the as-synthesized alumina nanorods exhibits a narrow band. The pore sizes are mainly distributed around 3.54 nm. From the corresponding isotherm (inset in Fig. 4), mesoporous Al_2O_3 is identified as a type IV isotherm with a hysteresis of type H1, revealing the existence of abundant mesoporous structures in the architectures. It was calculated that the as-synthesized alumina nanorods had a BET surface area about 176 m^2/g. The large surface area and narrow pore-size distribution combined with excellent thermal stability enhance the potential applications of these mesoporous alumina nanorods in catalysis.

The growth mechanism of AACH nanorods was proposed based on the surfactant-induced formation mechanism. Initially, the numerous AACH nanocrystals were formed through the following proposed reactions because of the homogeneous increase in pH in the system with urea decomposition [22].

$$CO(NH_2)_2 + H_2O \rightarrow CO_2 \uparrow + 2NH_3 \quad (4)$$

$$Al(NO_3)_3 + 4NH_3 + CO_2 + 3H_2O \rightarrow NH_4[Al(OOH)HCO_3] \downarrow + 3NH_4NO_3 \quad (5)$$

$$CO(NH_2)_2 + 3H_2O + CO_2 \rightarrow 2NH_4HCO_3 \quad (6)$$

Combining the above reactions yields an overall reaction:

$$Al(NO_3)_3 + 3CO(NH_2)_2 + 8H_2O \rightarrow NH_4[Al(OOH)HCO_3] \downarrow + 3NH_4NO_3 + 2NH_4HCO_3 \quad (7)$$

These AACH nanocrystals adsorbed on the PEG micelle via hydrogen bonding of the oxide groups of PEG with the OH groups of AACH [13], which was confirmed by the FTIR data shown in Fig. 5a. The strong bands at 3446 and 978 cm^{-1} are attributed to the stretching and bending vibrations of the hydroxyl groups on the AACH crystal surface, respectively [23]. The hydrogen bonding reduces the free energy of the AACH crystallites, which allows the AACH crystallites to grow into AACH/PEG nanorods along the direction of the axis of the rod-shaped copolymer micelles [24, 25]. Zhu et al. have interpreted the formation of the alumina nanofibers using a surfactant-induced fiber formation (SIFF) mechanism [13], which can also be applied to explain the formation of the AACH/PEG nanorods in our case. Also, the occlusion of PEG in AACH/PEG nanorods was confirmed by TGA and analysis FTIR data.

The formation of Al_2O_3 nanorods in the current synthesis system is further characterized by FTIR spectra, as shown in Fig. 5. The absorption bands at 1105, 978, 858, and 482 cm^{-1} belong to C–O–C and $–CH_2–$ vibration (Fig. 5a), which originate from surfactant of PEG, and the result suggests that some PEG molecules are absorbed onto the surface of AACH particles. The peaks in the region 3016–3174 cm^{-1} corresponded to symmetric bending stretching vibrations of NH_4^+, and around 1385 cm^{-1} is due to asymmetric bending modes. The bands at 1452 and 1539 cm^{-1} are ascribed to asymmetric stretching modes of CO_3^{2-}, the obvious split of this double degenerate peak exhibits that the CO_3^{2-} in the AACH belongs to the structural carbonate group. In the spectrum of calcined product shown in Fig. 5b, the three strong bands at 480, 633, and 749 cm^{-1} are ascribed to the vibration mode of AlO_6. The weak peak at 3444 cm^{-1} is due to asymmetric stretching mode of the adsorbed water from the air in the sample preparation process. The IR spectra of Al_2O_3 nanorods show that absorption peaks of carbonate, ammonium, and organic groups are greatly weakened, even vanishing in the range 1300–900 cm^{-1}, indicating complete decomposition of AACH and formation of alumina.

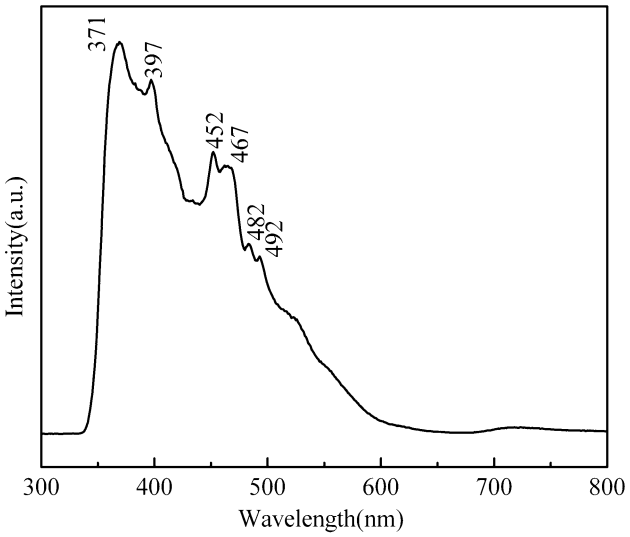

Fig. 6 Room temperature PL spectra of the as-prepared γ-Al_2O_3 nanorods

It is much significant to investigate the optical property of the as-prepared γ-Al_2O_3 nanorods since the chemical and physical properties of nanostructures strongly depend on their sizes and shapes. Figure 6 shows the room temperature PL spectra of γ-Al_2O_3 nanorods with an excitation of 325 nm. They are made up of several emission bands in a broad scope: one strong band at 370 nm, together with five weak shoulders located at 398, 452, 467, 482, and 493 nm. These emission bands may be attributed to the defect levels because the dangling bonds and unsaturated bonds on the surface of nanostructures are in favor of the formation of some additional energy levels in the wide-band gap crystals [26, 27]. Further insight into the optical property γ-Al_2O_3 nanorods is in progress.

Conclusions

In summary, we have reported, in this article, a facile route to prepare Al_2O_3 nanorods with hierarchically mesoporous structures by a hydrothermal and postcalcination approach. The ammonium aluminum carbonate hydroxide nanorods obtained by the hydrothermal method were used as the precursor, and converted to Al_2O_3 nanorods after thermal-decomposition treatment without the morphology deformation. The diameter of the Al_2O_3 nanorods is about $\sim$60 nm with a length about 1–2 μm, The N_2 adsorption–desorption experiment shows that the as-synthesized alumina nanorods have large surface area (ca. 176 m^2/g) and narrow pore-size distributions. On the basis of the experiment, we proposed a surfactant-induced nanorod formation mechanism by using the poly ethylene glycols micelles as the template agent for the nanorod assembly for the alumina nanorods with hierarchically mesoporous structures. We also conducted the photoluminescent test of γ-Al_2O_3 nanorods, which exhibits strong emission at room temperature.

Acknowledgments This study was supported by the National Science Foundation of China (No. 50772064), the Graduate Innovation Fund of Shaanxi University of Science and Technology and China Postdoctoral Science Foundation Founded Project (No. 20080440185).

References

1. Chandradass J, Balasubramanian M (2006) J Mater Sci 41:6026. doi:10.1007/s10853-006-0491-z
2. Tanada S, Kabayama M, Kawasaki N, Sakiyama T, Nakamura T, Araki M, Tamura T (2003) J Colloid Interface Sci 257:135
3. Bagshaw SA, Pinnavaia TJ (1996) Angew Chem Int Ed Engl 35:1102
4. Defriend AK, Barron RA (2003) J Mater Sci 38:2673. doi:10.1023/A:1024494821196
5. Zou JP, Pu L, Bao XM, Feng D (2002) Appl Phys Lett 80:1079
6. Li YW, Li N, Yuan RZ (1999) J Mater Sci 34:2547. doi:10.1023/A:1004636312836
7. Wang JH, Min BD, Lee JS et al (2004) Adv Mater 16:422
8. Rabin O, Herz PR, Lin YM, Akinwande AI, Cronin SB, Dresselhaus MS (2003) Adv Funt Mater 13:631
9. Zhao Q, Xu X, Zhang H, Chen Y, Xu J, Yu D (2004) Appl Phys A Mater Sci Process 79:1721. doi:10.1007/s00339-004-2911-8
10. Pu L, Bao XM, Zou JP, Feng D (2001) Angew Chem Int Ed 40:1490
11. Kwon SW, Park SB (2000) J Mater Sci 35:1973. doi:10.1023/A:1004774620783
12. Lee HC, Kim HJ, Rhee CH, Lee KH, Lee JS, Chung SH (2005) Micropor Mesopor Mater 79:61
13. Zhu HY, Riches JD, Barry JC (2002) Chem Mater 14:2086
14. Zhang Z, Pinnavaia TJ (2002) J Am Chem Soc 124:12294
15. Bai P, Su FB, Wu PP, Wang LK, Lee FY, Lv L, Yan ZF, Zhao XS (2007) Langmuir 23:4599
16. Cao MH, Wang YH, Guo CX et al (2004) J Nanosci Naonotech 4:824
17. Li ZQ, Xiong YJ, Xie Y (2003) Inorg Chem 42:8105
18. Hammond PT (2004) Adv Mater 16:1271
19. Li ZJ, Feng X, Yao HC et al (2004) J Mater Sci 39:2267. doi:10.1023/B:JMSC.0000017804.38298.92
20. Zhu ZF, Liu H, Sun HJ, Yang D (2009) Micropor Mesopor Mater 123:39
21. Wu ZS, Shen YD, Dong Y, Jiang JQ (2009) J Alloys Compd 467:600
22. Kara F, Sahin G (2000) J Eur Ceram Soc 20:689
23. Parida KM, Pradhan AC, Das J, Sahu N (2009) Mater Chem Phys 113:244
24. Jorgensen EB, Hvidt S, Brown W, Schillen K (1997) Macromolecules 30:2355
25. Ganguly R, Aswal VK, Hassan PA, Gopalakrishnan IK, Yakhmi JV (2005) J Phys Chem B 109:5653
26. Yu ZQ, Chang D, Li C, Zhang N, Feng YY, Dai YY (2001) J Mater Res 16:1890
27. Ma MG, Zhu YJ, Xu ZL (2007) Mater Lett 61:1812